Angular dependence of observed reflectances: A comparison with plane parallel theory

Norman G. Loeb[1]

Department of Atmospheric and Oceanic Sciences, McGill University, Montréal, Québec, Canada

Roger Davies

Institute of Atmospheric Physics, The University of Arizona, Tucson

Abstract. In this study, a direct comparison between plane parallel model calculations and one year of Earth Radiation Budget Satellite (ERBS) shortwave scanner observations over ocean between 30°S and 30°N is performed. Considering only cloud-contaminated pixels, plane parallel model calculations are first normalized to observations at nadir at high Sun elevations on a pixel-by-pixel basis by adjusting cloud fraction and cloud optical depth. These are then used to generate plane parallel model reflectances as a function of view, solar zenith, and relative azimuth angle, which are directly compared with the observations on a statistical basis. At moderate to high solar elevations ($\theta_0 \lesssim 63°$), the relative view angle dependence of plane parallel reflectances remains, on a statistical basis, within $\approx 10\%$ (relative difference) of that of the observations. For larger solar zenith angles, however, observed and plane parallel reflectances show systematic differences at all view angles that increase with increasing solar zenith angle. Provided atmospheric effects above the cloud are accounted for in the calculations, observed reflectances exceed plane parallel values in the backscattering direction by roughly a constant amount at all view angles for $\theta_0 \gtrsim 63°$. In the forward scattering direction, observed reflectances generally fall within the range of plane parallel model values (for a range of model assumptions) but show a very different view angle dependence; observed reflectances level off at view angles between 60° and 73°, whereas the calculations increase steadily. When stratified by pixel brightness, the plane parallel model generally provides a better approximation to the observed reflectance dependence on view angle for darker (i.e., optically thinner) pixels than for brighter (optically thicker) pixels. For the brightest pixels, reflectance differences are largest at nadir in the backscattering direction and at oblique view angles in the forward direction. Overall, the relative dependence on azimuthal angle is similar for the observations and plane parallel model, irrespective of cloud thickness. Neglecting pixel area expansion with view angle in the calculations is shown to have only a minor influence. Finally, the marked difference in the reflectance dependence on solar zenith angle between observations and calculations is suggested as the likely reason why the principle of directional reciprocity applied to satellite measurements breaks down at ERBS pixel scales.

1. Introduction

Retrieval of cloud properties and estimation of scene albedo from satellite measurements involving scanning radiometers require the use of angular algorithms or models which can relate measurements at a given view and relative azimuth to optical properties of the clouds being observed. The conventional approach relies on the plane parallel assumption which considers clouds to be (locally) one-dimensional and therefore horizontally invariant. However, ample theoretical evidence exists [e.g., *Busygin et al.*, 1973; *McKee and Cox*, 1974; *Aida*, 1977; *Davies*, 1978, 1984; *Bréon*, 1992; *Kobayashi*, 1993] which shows that reflectivities from nonplane parallel clouds can differ substantially from those assumed to be plane parallel. By comparison, relatively few observational studies are available to confirm this. Additional

[1]Now at College of Oceanic and Atmospheric Sciences, Oregon State University, Corvallis.

observational studies are now needed to determine the extent of these differences for general cloud conditions.

Loeb and Davies [1996] recently showed that application of the plane parallel model assumption to measurements of nadir reflectance leads to a strong bias in the retrieved cloud optical depth. This bias increases systematically with solar zenith angle and is more pronounced for thicker clouds. The cause was traced to a fundamental flaw in plane parallel theory applied to real clouds: the model shows a decrease in nadir reflectance with increasing solar zenith angle, whereas satellite measurements show the opposite behavior. On the basis of theoretical simulations, it was noted that the inability of the plane parallel model to account for three-dimensional cloud effects is the likely cause for this discrepancy, and further work is needed to fully explain this result.

The present study completes the comparison between observations and plane parallel theory started by *Loeb and Davies* [1996] by also examining the relative dependence of reflectance on view and relative azimuthal angle for different solar zenith angles. One year of Earth Radiation Budget Satellite (ERBS) scanner measurements equatorward of 30° over ocean, thereby encompassing a wide range of general cloud types, are again considered. One-dimensional (1-D) cloud optical depth and cloud fraction estimates from nadir observations are used to generate plane parallel model reflectances as a function of relative azimuthal, viewing, and solar zenith angles. The statistics from these distributions are directly compared with those of the observations for the same viewing geometries. In order to minimize the effect of the solar zenith angle bias in retrieved cloud optical depth, nadir observations at only moderate and high solar elevations are considered in deriving 1-D cloud optical depth distributions. Since the analyzed data set is very large, the statistical information content in the observations is highly significant. The absence of measured data to constrain the input variables in the analysis, especially the lack of information on the subpixel cloud fraction, is shown to be much less of a problem when the data are analyzed statistically, and consistent results are obtainable for a wide range of input assumptions.

In the comparisons, shortwave reflectance averages, relative frequency distributions, and averages over certain percentile intervals of the reflectance frequency distribution are considered. In order to demonstrate that pixel area expansion associated with the ERBS scanner is not a serious problem, comparisons are also carried out at a degraded resolution corresponding to the most oblique view angle bin. Finally, as an extension to a previous study by *Davies* [1994], in which observations were shown to violate directional reciprocity, we further examine the nature of this reciprocity breakdown by directly comparing reciprocal Sun and view angle pairs for both observations and plane parallel calculations.

2. Methodology

2.1. Analysis Approach

The basic approach used to compare the angular dependence in reflectance between plane parallel model and observations involves two steps. First, the plane parallel calculations are normalized to the observations at nadir on a pixel-by-pixel basis by inferring cloud fraction f and cloud optical depth τ_p (only cloud-contaminated scenes are considered). Each (f, τ_p) pair is then used as input to the plane parallel model to generate reflectances at off-nadir angles. Once 1 year of observations has been processed, the ensemble of plane parallel reflectances is directly compared with the observations at different solar, view, and relative azimuth angles. We chose 10 intervals of the cosine of the solar zenith angle μ_0 between 0 and 1, seven intervals of the cosine of the view angle μ between 0.3 and 1, and six relative azimuth ϕ intervals of width 30° between 0° and 180°. (Symmetry about the solar plane is assumed so that $\phi > \pi$ maps to $2\pi - \phi$.) Comparisons are restricted to $\mu > 0.3$ since beyond this point, the Earth does not entirely fill the ERBS scanner field of view (FOV).

As described in detail by *Loeb and Davies* [1996] (hereinafter referred to as LD), two different approximations are used to normalize the calculations. In the homogeneous pixel approximation ("hom"), each pixel is assumed to be completely cloud covered ($f = 1$), and cloud optical depth is inferred directly from the observed shortwave reflectance. In the inhomogeneous pixel approximation ("inhom"), plane parallel, broadband reflectances are represented by the sum of the clear and cloudy contributions from each pixel (LD, equation (2)). An estimate of subpixel cloud fraction f is made for each pixel by comparing the shortwave and longwave pixel radiances with predetermined clear and cloud radiance thresholds. An estimate of the cloud optical depth τ_p is then obtained by comparing the reflectance corresponding to the subpixel cloud area with look-up tables of plane parallel model cloud reflectance.

Ideally, it would be desirable to use all μ_0 bins to normalize the calculations at nadir. However, because large solar zenith angles produce spuriously high values of modeled τ_p [*Loeb and Davies*, 1996], these must be excluded, and normalization is therefore restricted to $\mu_0 > 0.45$ to avoid this effect. To reduce computational times, normalization is further restricted to the following three μ_0 bins: $\mu_0 = 0.5 - 0.6, 0.7 - 0.8$, and $0.9 - 1.0$. While the cloud optical depth bias still exists in these μ_0 bins for thick clouds, the effect is much less pronounced than at smaller μ_0.

In the plane parallel model calculations, cloud reflectances are obtained using the DISORT program of *Stamnes et al.* [1988]. The atmosphere is divided into the following four homogeneous vertical layers: a lower boundary layer, a cloud layer (with a fixed cloud top height), a tropospheric layer, and a stratospheric layer.

Both molecular and aerosol extinction above and below the cloud layer are accounted for (based on the LOWTRAN 7 model atmospheres). Reflection from the ocean surface below the cloud layer is determined using the Lambertian model with an albedo of 7%. Within the cloud layer, drop-size distributions are given by *Deirmendjian's* [1969] C.1 cloud model with single scattering properties calculated from the Mie code of *Bohren and Huffman* [1983] using the refractive indices of *Hale and Querry* [1973]. Look-up tables of cloud reflectance were determined for 24 optical depths (defined at a wavelength of 0.55 μm between 0.5 and 200, view and solar zenith angles between 0° and 89° (at a 5° resolution), and 19 relative azimuth angles between 0° and 180° (at a resolution of 10°). The wavenumber resolution was fixed at $\Delta\nu = 1000$ cm^{-1}, over the 4000 cm^{-1} to 34,000 cm^{-1} range.

Representative clear sky reflectances (R^{CLR} of LD, equation (2)) were obtained directly from 1 year of observations. In order to identify clear scenes, longwave radiance threshold estimates were first defined for each μ bin. At nadir, the clear sky longwave threshold value was inferred from pixels identified as clear by the ERBE maximum likelihood estimation technique [*Wielicki and Green*, 1989]. These accounted for the warmest 17% of all nadir observations. At off-nadir view angles, longwave thresholds were defined by assuming that the same relative frequency of clear pixels obtained at nadir occurs there. Thus, since 17% of all nadir pixels were identified as clear, longwave thresholds at off-nadir view angles were inferred so as to also isolate the warmest 17% of the pixels. Then, by analyzing the shortwave reflectance frequency distributions of pixels with longwave radiances larger than the longwave thresholds, representative clear sky reflectances were defined at each angle from the peak reflectances in the shortwave reflectance frequency distributions. In this manner, representative clear sky reflectances were derived for 10 values of μ_0 between 0 and 1, seven values of μ between 0.3 and 1, and 18 values of ϕ between 0° and 180°.

Since the pixel area viewed by ERBS increases from approximately 1500 km^2 at nadir to 27,300 km^2 at a view angle of 70°, the above assumption that the relative frequency of clear pixels is the same at all view angles may not be strictly correct. As the pixel area increases, the fraction of clear pixels should decrease since larger pixels have a greater likelihood of at least some cloud contamination than smaller pixels. *Ye and Coakley* [1996b] estimated that the frequency of clear pixels decreased from approximately 17% at nadir to 8% at view angles between 63° and 75°. To examine this, clear sky reflectances inferred from reflectance frequency distributions for the warmest 17% of all pixels falling in the most oblique μ bin were compared with those obtained for the warmest 8% of all pixels. Overall, while the frequency distributions showed some differences, the peak reflectances (and therefore the clear

sky reflectance values) did not change very much; absolute differences at all μ_0 and ϕ were generally less than 1%.

2.2. Error Analysis

Since 1 year of observations is considered, the μ bins are generally well sampled. Uncertainties in the mean observed shortwave reflectance are typically less than 0.5% (absolute reflectance) at all angles except close to the forward scattering peak ($\phi = 0°$), where the number of samples is much smaller. When indicated, error bars in the graphs in section 3 are derived using equation (5) of LD.

In contrast, the model calculations are associated with larger uncertainties. For this reason, a number of different plane parallel model calculations are considered, encompassing a wide range of model assumptions. One of the largest uncertainties in the plane parallel calculations involves the specification of cloud fraction—cloud optical depth pairs used to normalize the plane parallel calculations at nadir. While different combinations can yield the same reflectance at nadir, the corresponding angular reflectance dependence varies substantially. In order to account for these uncertainties and to ensure that any differences between the observations and plane parallel calculations are not simply due to uncertainties in normalization, both the inhomogeneous and homogeneous pixel approximations are considered. Also, three different approximations for the contribution from the clear sky above the cloud top are employed ($Z_t = 3$ km, 6 km, and the case where clear sky effects are neglected). Since the model calculations account for scattering by water clouds only while the observations encompass all cloud types including ice clouds, additional comparisons are carried out with and without the inclusion of thick ice clouds in the analysis. These scenes are identified by removing the coldest 10% of all samples (described in LD).

The increase in ERBS pixel area with view angle introduces another uncertainty since this is not accounted for in the plane parallel calculations. Rather, off-nadir reflectances are calculated at the same resolution as at nadir (where the calculations are normalized). A separate analysis is therefore performed in section 3.4, in which we repeat the observed versus 1-D model comparisons using data which have been degraded to a constant spatial resolution in all μ bins, equal to that at $\mu = 0.35$ (the midpoint of the most oblique μ bin).

Other uncertainties in the calculations include variations in cloud microphysics, uncertainties caused by the use of a coarse spectral resolution in the broadband reflectances ($\lesssim 3$%), and uncertainties in ocean surface reflectance contributions from below the cloud layer. These latter uncertainties are found to be much smaller, however. The largest of these is due to cloud microphysics, which causes a relative uncertainty of less than 5% at all μ, based on comparisons between the

C.1 cloud model (effective radius of 6 μm) and a cloud model having an effective radius of 10 μm.

3. Observed versus Plane Parallel Model Comparisons

3.1. View Angle Dependence

To examine the sensitivity in average observed shortwave reflectance to inclusion/exclusion of thick ice clouds, clear scenes, and to pixel area expansion, Figures 1a and 1b show observed shortwave reflectance averages as a function of μ for $\mu_0 = 0.1 - 0.2$ and $0.7 - 0.8$, respectively, in the back ($\phi = 120° - 180°$) and forward ($\phi = 30° - 60°$) scattering directions. The $\phi = 0° - 30°$ interval was excluded to avoid sun glint and because sample sizes are smaller there. In Figure 1, mean reflectances from all observations throughout the year ("all obs") are compared with those obtained when clear sky pixels are excluded ("no clr"), when both clear

sky pixels and pixels consisting of thick ice clouds are excluded ("no clr/cirr"), and when the data are degraded to a constant spatial resolution at all μ equal to that at $\mu = 0.35$ ("degr (no clr)"). As shown, when only clear scenes are excluded, the average reflectance increases by $\approx 10 - 15\%$ (relative increase), but little change is observed in the relative μ dependence. If scenes consisting of thick ice clouds are also removed, this reduces the average shortwave reflectances to values comparable to the all observations case. When the observations are degraded to a constant spatial resolution at all μ (degr (no clr)), the average shortwave reflectance decreases by $\lesssim 5\%$ (relative difference) at nadir compared to the no clr case at full resolution. Thus, while the average observed shortwave reflectance shows some sensitivity to the manner in which observations are averaged, this sensitivity is weak and does not have much influence on the shortwave reflectance dependence on μ.
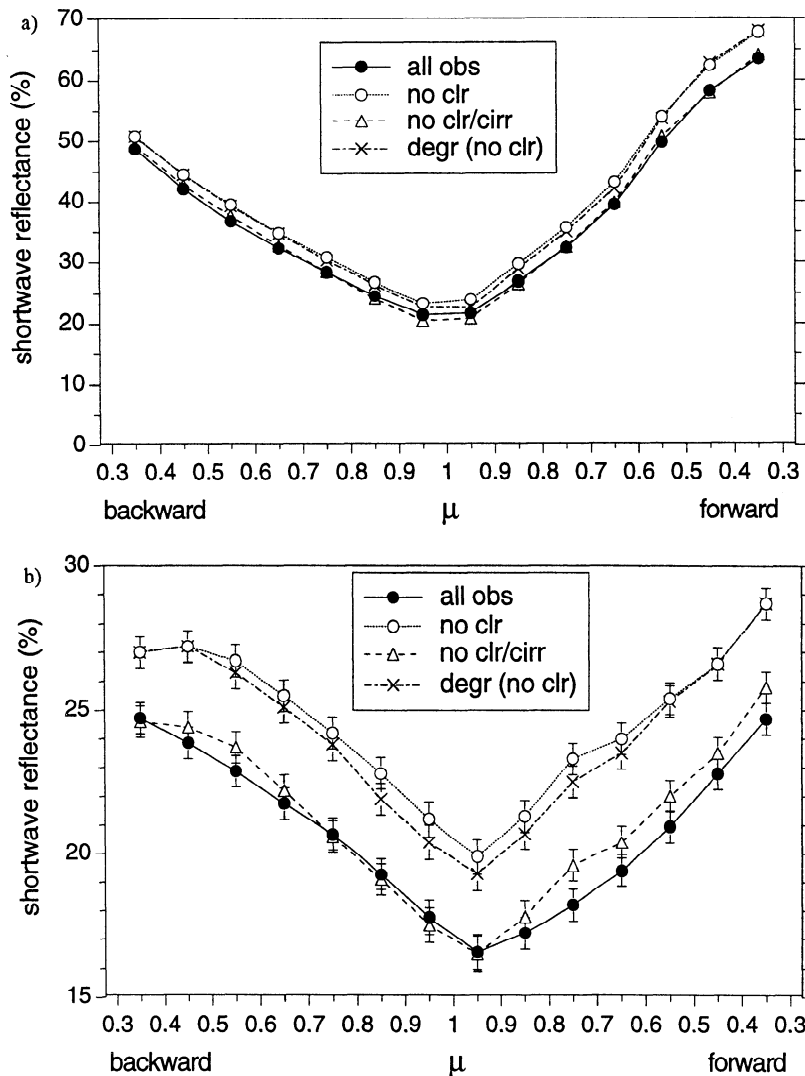

Figure 1. Observed shortwave reflectance averages as a function of cosine of view angle μ in the backscattering direction (relative azimuth $\phi = 120° - 180°$) and in the forward scattering direction ($\phi = 30° - 60°$) for (a) cosine of solar zenith angle $\mu_0 = 0.1 - 0.2$ and (b) $\mu_0 = 0.7 - 0.8$.
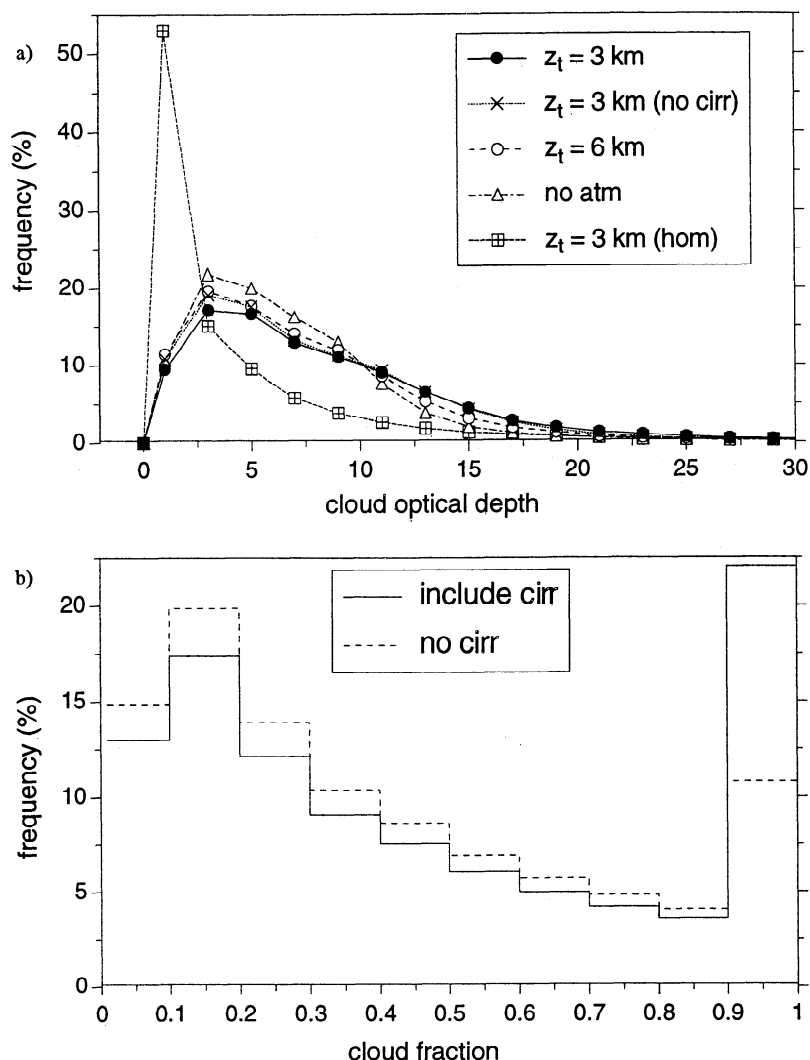
Figure 2. (a) Cloud optical depth and (b) cloud fraction distributions inferred from the normalization of the plane parallel calculations from nadir observations at $\mu_0 = 0.5 - 0.6$, $0.7 - 0.8$, and $0.9 - 1.0$. "$Z_t = 3$ km" refers to the case where a cloud top height of 3 km is used, "$Z_t = 6$ km" is for a cloud top height of 6 km, "no atm" is for the case where the clear sky above the cloud is neglected, "$Z_t = 3$ km (hom)" refers to the homogeneous pixel approximation for a cloud top at 3 km, and "$Z_t = 3$ km (nocirr)" refers to a cloud with $Z_t = 3$ km, in which thick ice clouds are excluded from the analysis.

Figure 2a shows cloud optical depth distributions obtained after normalizing the plane parallel model calculations to nadir observations at $\mu_0 = 0.5 - 0.6$, $0.7 - 0.8$, and $0.9 - 1.0$. Results for the inhomogeneous approximation under three different assumptions for the clear sky contribution above the cloud (i.e., "$Z_t = 3$ km", "$Z_t = 6$ km", and "no atm") and a case where thick ice clouds are excluded ("$Z_t = 3$ km (no cirr)") are provided, together with results for the homogeneous pixel approximation with $Z_t = 3$ km ("$Z_t = 3$ km (hom)"). As shown, the largest influence on the cloud optical depth distribution is determined by whether the inhomogeneous or homogeneous pixel approximation is used. Since all pixels are assumed to have a cloud fraction of unity in the latter case, the frequency of very thin clouds is much larger. The average cloud optical

depth is 5.4 ($Z_t = 3$ km (hom)), compared with 9.5 for the inhomogeneous approximation ($Z_t = 3$ km). As cloud top height increases, attenuation above the cloud decreases and inferred cloud optical depths decrease; average cloud optical depths for the $Z_t = 6$ km and no atm cases are 7.8 and 6.8, respectively. For the $Z_t = 3$ km (no cirr) case, the average is 7.6.

Figure 2b shows cloud fraction frequency distributions obtained when thick ice clouds are included ("include cirr") and excluded ("no cirr") from the analysis. Compared with the cloud optical depth distributions in Figure 2a, a much stronger sensitivity to the presence/absence of thick ice clouds is observed; the frequency of overcast pixels almost doubles when the thick ice clouds are included.

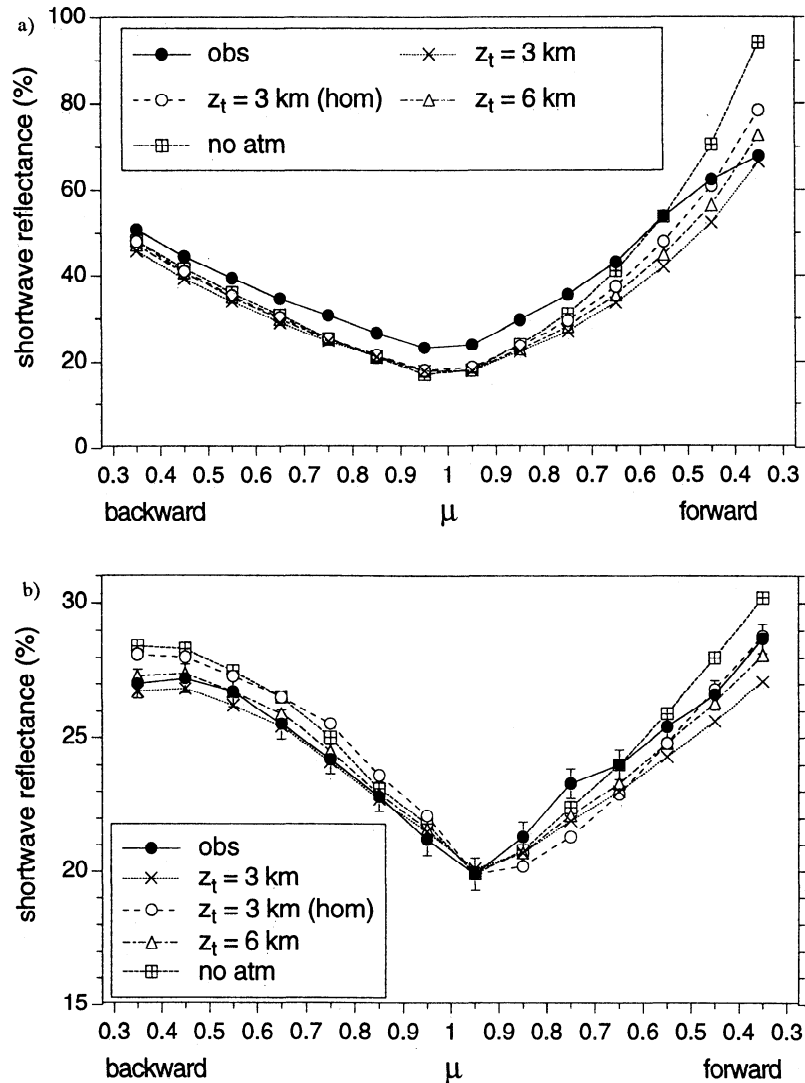Average shortwave reflectances calculated using the

Figure 3. Average shortwave reflectances for the observations and calculations as a function of μ for (a) $\mu_0 = 0.1 - 0.2$ and (b) $\mu_0 = 0.7 - 0.8$.

cloud fraction—cloud optical depth distributions in Figure 2 are compared directly with the observations (excluding clear pixels) in Figures 3a and 3b for $\mu_0 = 0.1 - 0.2$ and $0.7 - 0.8$, respectively. In both cases, the same ϕ intervals as in Figure 1 are used. For $\mu_0 = 0.7 - 0.8$, plane parallel reflectances match the observations closely. Relative differences are generally less than $\approx 5\%$. At $\mu_0 = 0.1 - 0.2$, the overall μ dependence for the plane parallel model is qualitatively consistent with the observations in the backscattering direction, but the observations are noticeably larger. In the forward scattering direction, the observations generally fall within the range of plane parallel model values for $\mu < 0.65$ but show a very different μ dependence; observed reflectances level off between $\mu = 0.5$ and 0.3, whereas the calculations show a steady increase.

Figure 3 also clearly illustrates the sensitivity of the average calculated reflectances to the model assumptions. While the sensitivity is small at nadir, it becomes

larger as μ decreases, especially for the no atm and $Z_t = 3$ km cases in the forward direction (Figure 3a). By comparison, the sensitivity in the backscattering direction is much smaller. When an atmosphere is inserted above the cloud, reflectance at the top of the atmosphere (TOA) decreases substantially in the forward scattering direction because cloud reflectance, which is very large owing to the forward peak in the cloud scattering phase function, is attenuated by the atmosphere. It is most pronounced at small μ because of the large path length scattered radiation must travel through before reaching the TOA. Adding an atmosphere also contributes radiation at the TOA by directly scattering solar radiation (above the cloud) and redirecting upwelling diffuse radiation from the cloud into the satellite FOV. These have a larger relative contribution in the backscattering direction, however, because cloud reflectance is much smaller there. In fact, the decrease in TOA reflectance due to atmospheric attenuation in
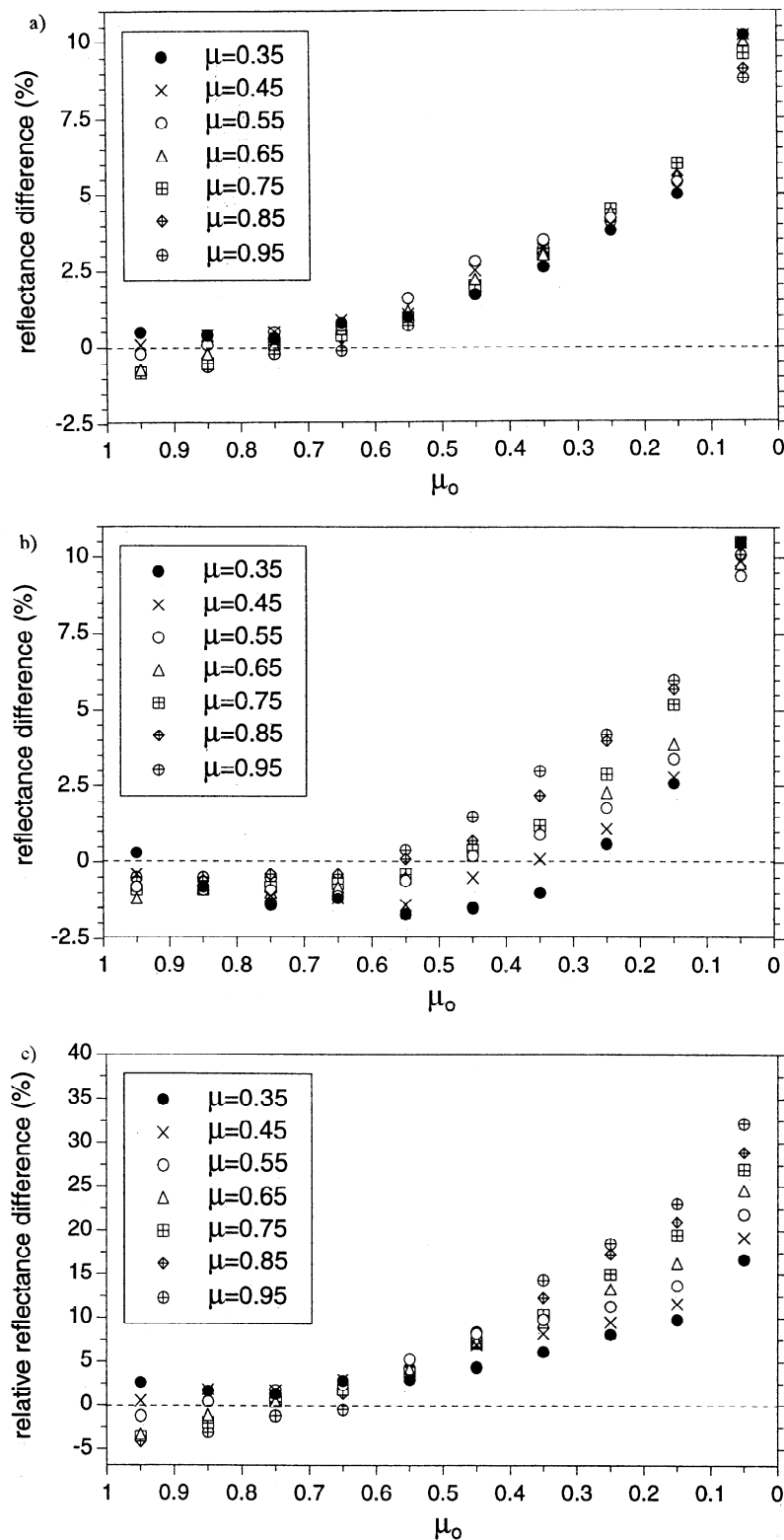
Figure 4. Reflectance differences between the observed and calculated reflectances as a function of μ_0 and μ in the backscattering direction for (a) $Z_t = 3$ km and (b) no atm and (c) relative differences for $Z_t = 3$ km.

the backscattering direction is largely compensated by the atmospheric scattering contribution. Consequently, sensitivity to the atmosphere is much more pronounced in the forward scattering direction.

Figures 4a and 4b show the absolute difference in

average reflectance between the observations and calculations in the backscattering direction as a function of μ_0 and μ for the $Z_t = 3$ km and the no atm cases, respectively. Only the backscattering results are shown because sensitivity to model assumptions is smaller in
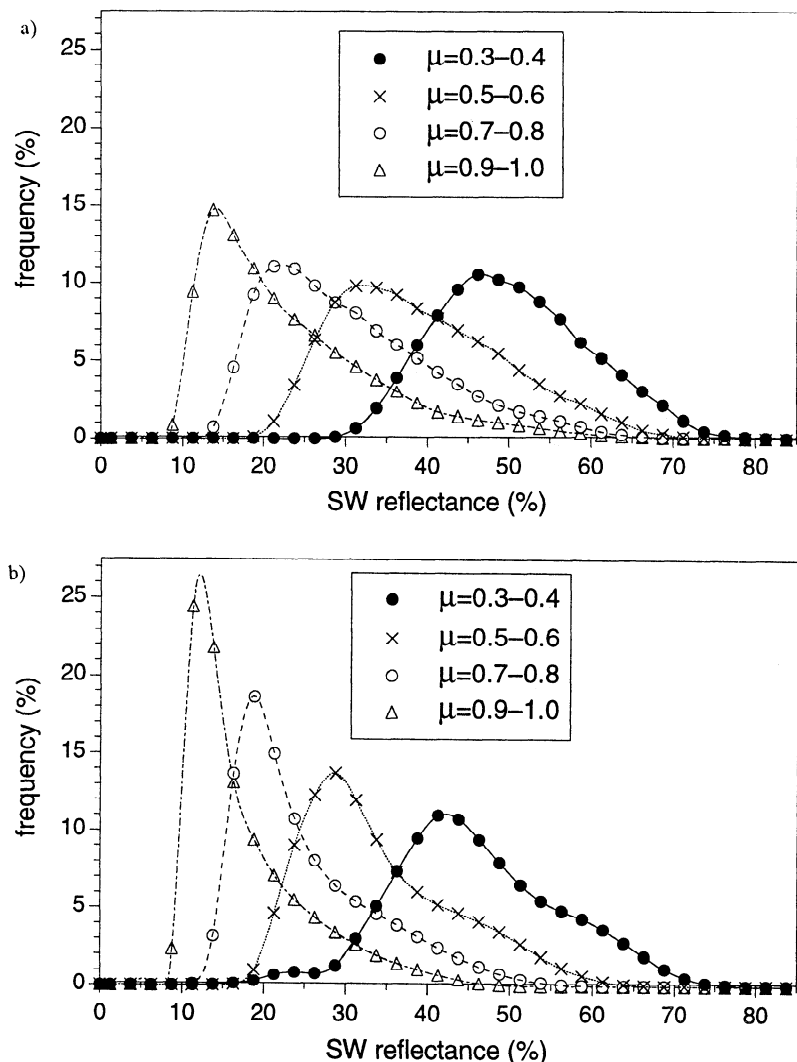
Figure 5. (a) Observed and (b) calculated reflectance frequency distributions as a function of μ for $\mu_0 = 0.1 - 0.2$ in the backscattering direction.

that direction. For $\mu_0 > 0.45$, plane parallel reflectances are generally consistent with the observations at all μ. As μ_0 decreases, differences increase, reaching $\approx 10\%$ (absolute reflectance) at $\mu_0 = 0.0 - 0.1$. Thus the μ_0 reflectance bias observed at nadir by *Loeb and Davies* [1996] also affects off-nadir reflectances as well. Interestingly, for the $Z_t = 3$ km case (Figure 4a), there is no systematic μ dependence in the differences. Rather, reflectance differences increase by the same amount at all μ as μ_0 decreases. When the atmosphere above the cloud is neglected (Figure 4b), a much stronger μ dependence is observed; differences tend to be larger at nadir than at oblique view angles. Thus, while inclusion of atmospheric effects may lead to larger reflectance errors at small μ, it nonetheless provides a μ dependence in average reflectance that is closer to that of the observations (therefore removing any μ-dependent bias). Because average reflectance increases with decreasing μ while absolute differences show less variability, relative reflectance differences inevitably increase with μ, as il-

lustrated in Figure 4c. On average, relative errors in the backscattering direction are $\lesssim 20\%$ for $\mu \lesssim 0.5$ and increase with μ.

The absence of a strong μ dependence in the absolute difference between average observed and plane parallel model reflectances in the backscattering direction is surprising. *Minnis* [1989] showed that when cloud amounts were examined at different view angles using collocated Geostationary Operational Environmental Satellite (GOES) west and GOES east radiances, the cloud amounts tended to increase with view angle. While the low spatial resolution of the ERBS scanner and the fact that the measurements are broadband may play a role, it is unlikely that these would change this basic result. In another study, *Coakley* [1991] used high-resolution (1 km) monochromatic measurements from the advanced very high resolution radiometer (AVHRR) to compare the anisotropy of 0.63 μm radiation reflected by uniform and broken stratocumulus cloud layers off the coast of California during the
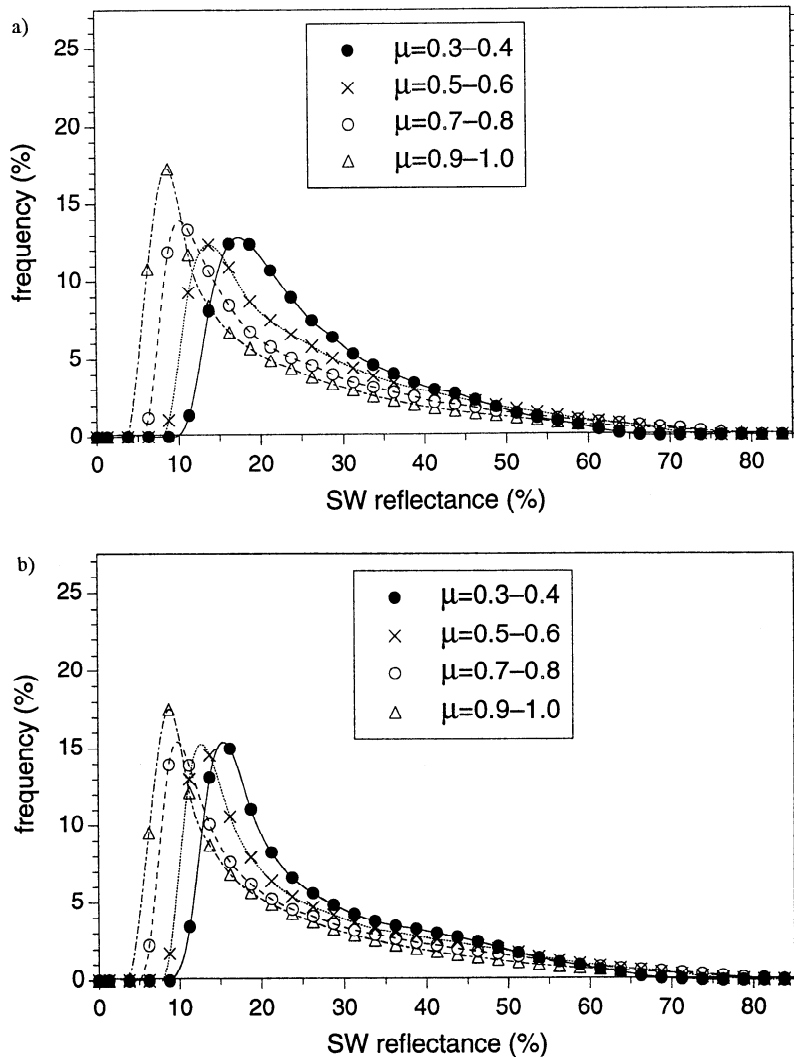
Figure 6. (a) Observed and (b) calculated frequency distributions of reflectance as a function of μ for $\mu_0 = 0.7 - 0.8$ in the backscattering direction.

3 week period of the First International Satellite Cloud Climatology Project (ISCCP) Regional Experiment Intensive Field Observations (FIRE). For the range of μ_0 considered ($\mu_0 = 0.4 - 0.65$ and $0.7 - 0.9$), differences in reflectance between uniform and broken cloud layers showed no change with μ. Unfortunately, they did not perform any comparisons at smaller μ_0. In another study, *Rossow* [1989] found similar results. In that case, the ISCCP radiative model (which represents clouds as single, homogeneous layers over scales of 4 to 16 km) was used to infer cloud optical depths from 1 month of collocated Meteosat 2 and GOES 5 east scenes viewed by each satellite at different μ. Differences in cloud optical depth retrievals as a function of the difference in μ for the two satellites were shown to be small. Unfortunately, it was not mentioned what solar zenith angles were considered, results were not stratified by relative azimuth, and the comparisons included a number of land scenes (enough to cause a noticeable bias in visible radiance differences).

Figures 5 and 6 show the observed and calculated ($Z_t = 3$ km) reflectance frequency distributions in the backscattering direction corresponding to the mean reflectances in Figures 3a and 3b, respectively. At $\mu_0 = 0.1 - 0.2$ (Figure 5), observed and calculated reflectance frequency distributions look quite different at nadir. While the peak reflectance occurs at roughly the same point, the observed reflectance distributions are much broader in appearance and show a much smaller frequency close to the peak reflectance than do the plane parallel results. In contrast, the shape of the observed and calculated reflectance distributions look remarkably similar at small μ. Despite this similarity, however, the peak reflectances are not the same. For example, the peak in the observed reflectance distribution at $\mu = 0.3 - 0.4$ (Figure 5a) occurs at $\approx 47\%$, whereas the corresponding calculated reflectance peak occurs at $\approx 42\%$ (Figure 5b). Thus, while the difference between observed and calculated average reflectance shows little sensitivity to μ for the $Z_t = 3$ km case, a larger
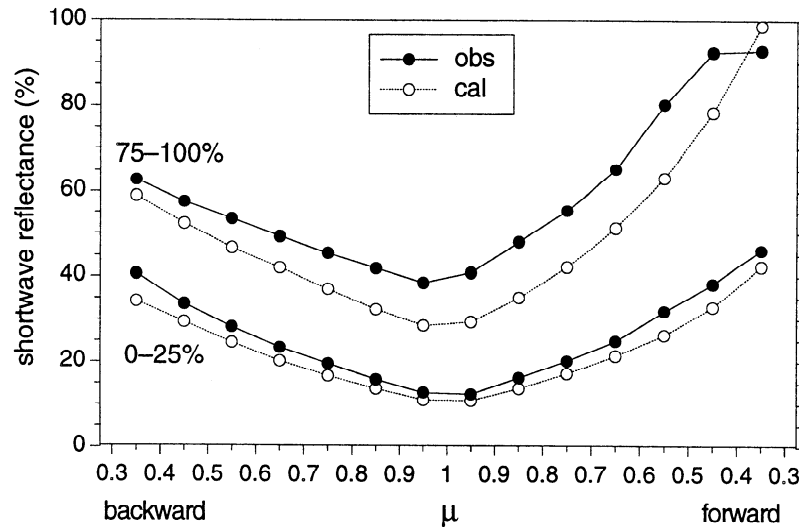
Figure 7. Observed and calculated reflectance averages for reflectances lying between the 0−25% and 75 − 100% percentile invervals for $\mu_0 = 0.1 - 0.2$.

sensitivity is apparent in the reflectance frequency distributions. In contrast, at $\mu_0 = 0.7 - 0.8$ (Figures 6a and 6b), the observed and plane parallel reflectance frequency distributions are quite similar at all μ.

3.2. Dependence on Pixel Brightness

At the ERBS pixel scale, it is clear from Figure 2b that most of the pixels in our data set are partially cloud contaminated. On average, pixels having low cloud fractions (and cloud optical depths) will be darker, while the reverse will be generally true for pixels with large cloud fractions (and cloud optical depths). In order to examine how calculations and observations compare for these cases, Figure 7 shows average shortwave reflectances corresponding to two reflectance classes of occurrence derived from the underlying observed and calculated reflectance frequency distributions at $\mu_0 = 0.1 - 0.2$ for the $Z_t = 3$ km case. For the darkest pixels (0 − 25% percentile interval), the plane parallel reflectances are in good agreement with the observations (relative reflectance differences $\lesssim$ 15%). For the brightest pixels (75 − 100% percentile interval), reflectance differences in the backscattering direction are largest at nadir and decrease with decreasing μ. Differences are also large in the forward direction, and there is a tendency for reflectances to level off at the most oblique view angles. Thus, from these results, it appears that the 1-D model provides a better approximation for optically thinner pixels.

To examine these results more closely, Figures 8a and 8b show differences between observed and plane parallel reflectances in various percentile intervals for the inhomogeneous approximation with $Z_t = 3$ km and 6 km, respectively. In the backscattering direction, both cases show the reflectance difference to be least sensitive to pixel brightness at oblique view angles (relative differ-

ence $\lesssim$ 15%) and most sensitive at nadir. Consequently, reflectance differences increase slightly with decreasing μ for the darkest 25% of the cases, show a smaller variability for the intermediate classes (e.g., 25 − 50% and 50 − 75%), and decrease for the 75 − 100% class. The lack of a strong dependence at oblique view angles results from the fact that the shapes of the observed and calculated reflectance frequency distributions are so similar at small μ (Figure 5). In contrast, since the nadir observed frequency distribution has a much higher frequency of large reflectances, differences tend to be greater for the brightest pixels.

In the forward scattering direction, reflectance differences show a larger sensitivity to pixel brightness. For $\mu > 0.5$, differences increase slightly with decreasing μ and then suddenly decrease at very oblique view angles. In fact, for the brightest pixels, plane parallel reflectances exceed the observations at $\mu = 0.3 - 0.4$ in both Figures 8a and 8b. Differences are especially large when clear sky attenuation above the cloud is small; the calculations exceed the observations by as much as 20% (Figure 8b). When reflectance differences are compared for different percentile intervals at $\mu_0 = 0.7 - 0.8$ (not shown), no appreciable dependence on pixel brightness is observed, and relative differences remain less than ≈5% at all μ.

3.3. Relative Azimuth Dependence

Figure 9a compares average observed and plane parallel reflectances as a function of relative azimuth ϕ for $\mu_0 = 0.1 - 0.2$ at $\mu = 0.3 - 0.4$. Errors in mean observed reflectance are larger in certain ϕ bins owing to reduced sampling and because a smaller bin size was used in this comparison (10° instead of 30°). Overall, the plane parallel model appears to provide a reasonable representation of the observed ϕ dependence. In the forward
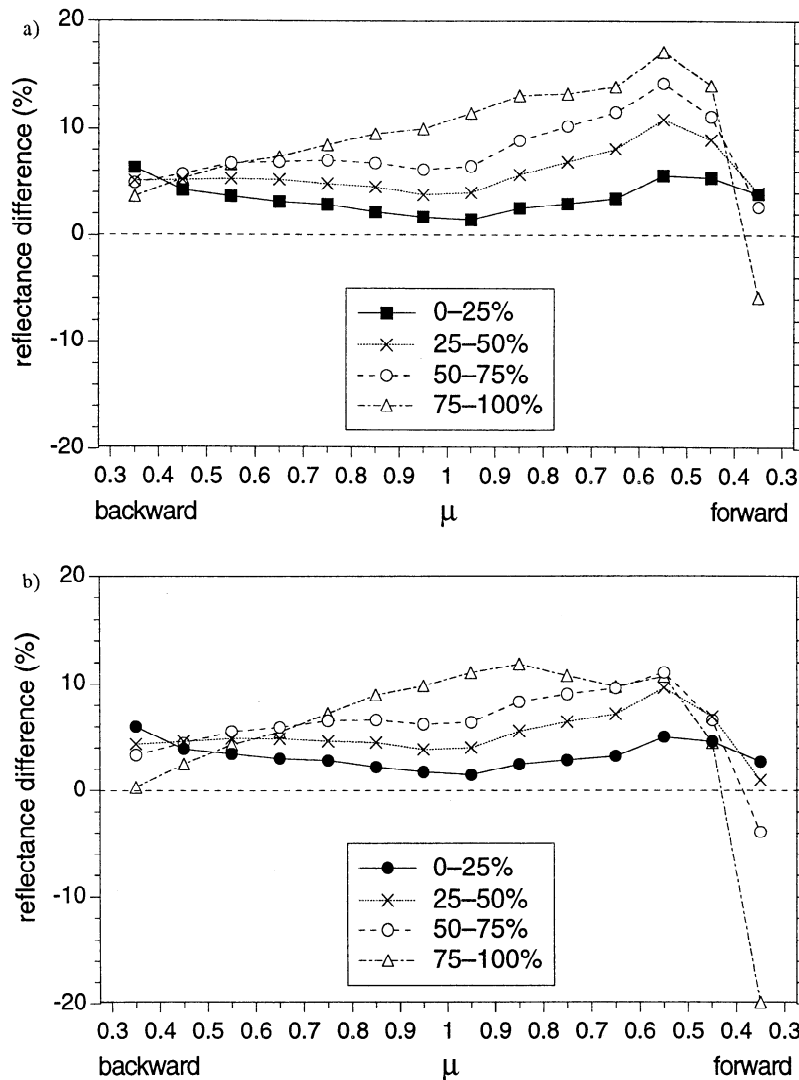
Figure 8. Reflectance differences between the observations and calculations at $\mu_0 = 0.1 - 0.2$ for the inhomogeneous pixel approximation with a cloud top height of (a) 3 km and (b) 6 km.

scattering direction, both observed and plane parallel model reflectances increase rapidly with decreasing ϕ, and the observations fall well within the range of values provided by the plane parallel model. Sensitivity to the clear sky above the cloud and to the type of approximation used in normalizing the calculations (i.e., either "inhomogeneous" or "homogeneous") is also clearly illustrated. For $\phi < 70°$, the calculations appear to be more sensitive to attenuation by the atmosphere above the cloud than to the details of the normalization procedure.

In the side and backscattering directions, the ϕ dependence in the calculations is also fairly similar to that observed, regardless of model assumptions. The largest differences occur for $70° < \phi < 140°$ and for $170° < \phi < 180°$, where observed reflectances are approximately 6% larger than plane parallel values ($\approx 15\%-20\%$ relative difference). For $140° < \phi < 170°$, differences are generally less than 3% ($\approx 6\%$ relative difference).

For $\mu = 0.7-0.8$, Figure 9b shows that the plane parallel model successfully captures the relative azimuthal dependence of the observations but that it is systematically biased. Observations exceed the calculations by a constant amount of $\approx 6\%$ at all ϕ in the backscattering direction ($\approx 20\%$ relative difference), and a fairly similar ϕ dependence is also observed in the forward direction.

3.4. Pixel Area Expansion

To examine whether the neglect of pixel area expansion in the calculations affects these results, comparisons between observations and calculations were also made after degrading the data in each viewing direction to a constant spatial resolution equal to that at $\mu = 0.35$ [after *Ye and Coakley*, 1996a]. The data are degraded by averaging reflectances from an appropriate number of neighboring pixels whose combined area matches that of a single pixel at $\mu = 0.35$. The analysis accounts for
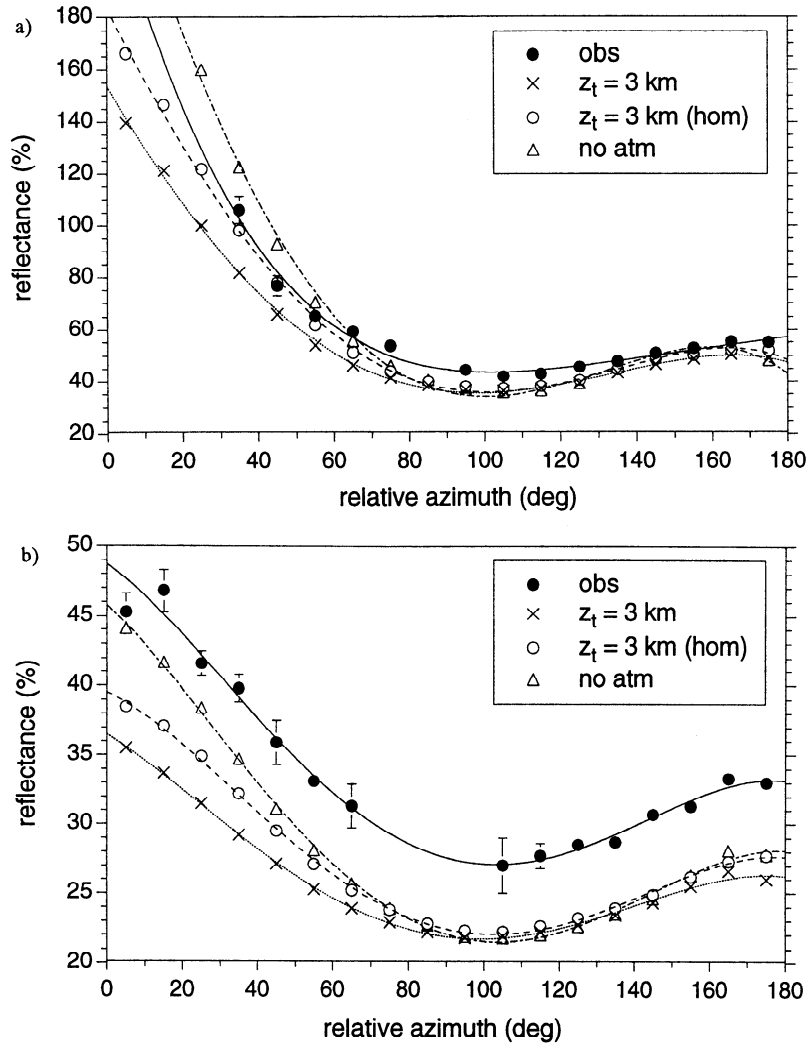
Figure 9. Average observed and plane parallel reflectances as a function of relative azimuth for $\mu_0 = 0.1 - 0.2$ at (a) $\mu = 0.3 - 0.4$ and (b) $\mu = 0.7 - 0.8$.

the approximate 35% overlap in neighboring ERBS pixels [*Kopia*, 1986]. Table 1 shows the number of pixels in each μ bin used to construct the constant FOVs, along with their combined total area ("simulated pixel area"), and the relative difference from the actual pixel area at $\mu = 0.35$. As shown, relative differences between the simulated pixel areas and the actual ERBS pixel area at $\mu = 0.35$ are less than 10%.

Figures 10a and 10b show the cloud fraction and cloud optical depth frequency distributions, respectively, at the full and degraded pixel resolutions. Figure 10a further stratifies these comparisons to include or exclude clear pixels from the analysis. In general, differences between the full and degraded resolution cloud fraction frequency distributions tend to be small. Degrading the pixel resolution causes only a slight

Table 1. Number of Earth Radiation Budget Satellite Pixels in Each View Angle μ Bin Required to Construct Fields of View of Constant Area Equal to the ERBS Pixel Resolution at $\mu = 0.35$

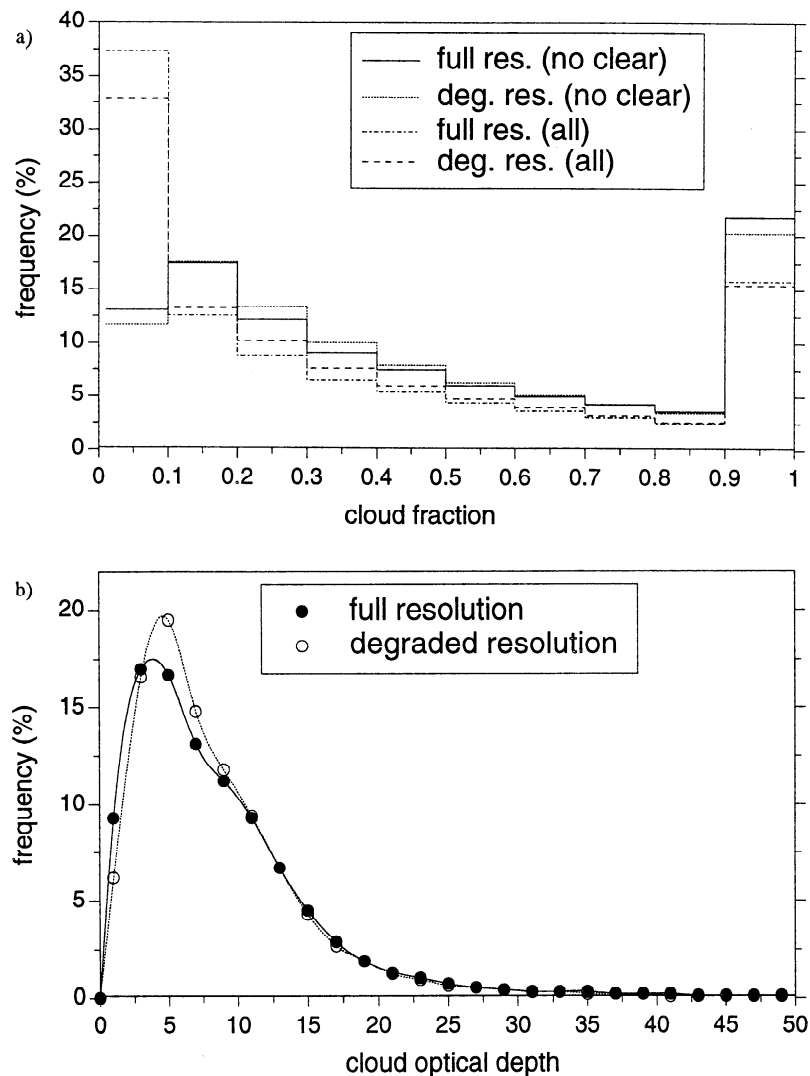| μ Bin	Number of Pixels	Simulated Pixel Area, km^2	Simulated Pixel Area Error, %
0.35	1	25,782.9	0.0
0.45	2	23,580.5	−8.5
0.55	3	23,588.5	−8.5
0.65	7	25,573.1	−0.8
0.75	11	26,175.8	1.5
0.85	16	26,217.9	1.7
0.95	20	23,829.5	−7.6

Figure 10. Frequency distributions obtained from nadir observations for the full and degraded pixel resolutions showing (a) cloud fraction and (b) cloud optical depth.

reduction in the frequency of very small ($f = 0.0 - 0.1$) and very large ($f = 0.9 - 1.0$) cloud fractions. These differences are much smaller than those observed in studies involving high-resolution sensors [*Wielicki and Parker*, 1992]. Differences between full and degraded resolution cloud optical depth frequency distributions are also found to be slight (Figure 10b); average cloud optical depths for these cases are 9.4 for the full resolution case and 8.9 for the degraded resolution case.

Shortwave reflectance frequency distributions at $\mu_0 = 0.1 - 0.2$ and $0.7 - 0.8$ for both the full and degraded resolution observations and calculations are provided in Figures 11a and 11b, respectively. As shown, degrading the pixel resolution has very little effect. Overall, relative differences between full and degraded resolution reflectance standard deviations are less than 10%.

While the influence of pixel area expansion may be small when compared with a constant ERBS pixel size at $\mu = 0.35$, it is not immediately clear how these results would change if a smaller constant FOV size,

such as that corresponding to pixels at nadir, were used at all μ. Unfortunately, this cannot be examined using ERBS data alone but would require measurements from a higher-resolution sensor (e.g., AVHRR). In all likelihood, this would probably result in a stronger increase in reflectance with decreasing μ since cloud-contaminated scenes viewed obliquely would generally contain more cloud within the pixels. However, if the sensitivity to pixel resolution at small μ is at all similar to that shown in Figure 11 for $\mu = 0.9 - 1.0$, the magnitude of any such changes would likely be small.

3.5. Directional Reciprocity Applied to ERBS Measurements

Because of limitations associated with orbit-dependent sampling biases inherent in satellite measurements, there is often a need in remote sensing applications to "fill in" missing or unreliable data in certain view and solar zenith angle bins by using empirical or theoretical techniques. This problem often arises at very oblique
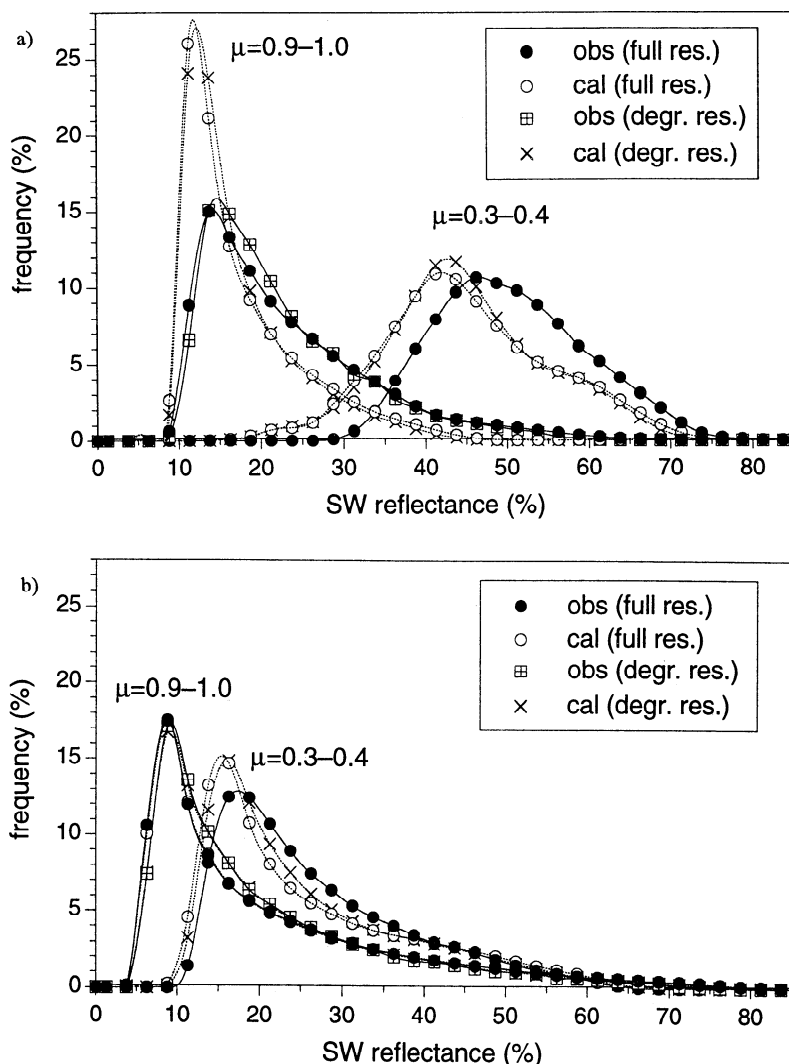
Figure 11. Shortwave reflectance frequency distributions for the full and degraded resolution observations and calculations in the backscattering direction for (a) $\mu_0 = 0.1 - 0.2$ and (b) $\mu_0 = 0.7 - 0.8$.

view angles (e.g., $\mu < 0.3$), where satellite measurements may be less dependable, and at low Sun elevations, where data are often missing. In the latter case, the problem is typically encountered when measurements are taken from instruments in Sun-synchronous orbits, where there is a high degree of correlation between solar zenith angle and latitude.

A common theoretical approach used in dealing with this problem is a simplified version of the Helmholtz principle of reciprocity. For a (locally) one-dimensional horizontally homogeneous medium, the general Helmholtz principle of reciprocity reduces to a simple directional principle, given by the reciprocal relation $R_A(\mu_A, \phi_A; \mu_B, \phi_B) = R_B(\mu_B, \phi_B; \mu_A, \phi_A)$, where R_A is the reflectance in the direction (μ_A, ϕ_A) due to insolation from the direction (μ_B, ϕ_B) and vice versa for R_B [*Chandrasekhar*, 1950]. Thus, if measurements are missing in certain angular bins, measurements from the corresponding reciprocal incident and view angle bins can be used to fill in the missing data.

Since satellite measurements are actually averages over the spatial scale of a pixel, this special case of the general principle of reciprocity requires the scene to be horizontally homogeneous over the pixel scale. In this context therefore we can interpret the principle of directional reciprocity as a necessary (but not sufficient) condition for the application of plane parallel theory to the analysis of real measurements [*Davies*, 1994]. If observations violate directional reciprocity, then direct application of 1-D theory to real measurements would be inappropriate and the general principle of reciprocity would have to be considered. In order to test whether or not real measurements satisfy directional reciprocity, *Davies* [1994] compared autocorrelation functions for reciprocal pairs of reflected shortwave radiances measured by the ERBS scanner for April-July 1985 within 30° of the equator. When autocorrelations at zenith Sun as a function of μ were compared with those measured at nadir as a function of μ_0, differences tended to be large when clouds were present but were small
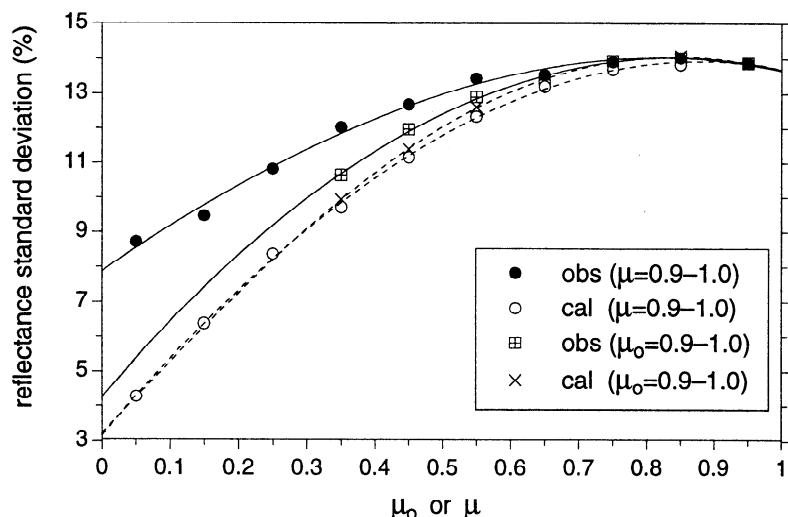
Figure 12. Observed and plane parallel model reflectance standard deviations for the reciprocal sets of angles $\mu = 0.9 - 1.0$ as a function of μ_0 and $\mu_0 = 0.9 - 1.0$ as a function of μ in the backscattering direction.

for clear scenes. As a result, it was concluded that directional reciprocity does not apply at the ERBS pixel resolution owing to inherent horizontal inhomogeneities in the cloud field at that spatial scale.

It is not immediately clear from that study how these horizontal inhomogeneities affect the reflection field. For example, is directional reciprocity violated because horizontal inhomogeneities cause the μ dependence in reflectance to change (compared to 1-D theory), or is it because of their effect on the μ_0 dependence and thus the scene illumination? To gain more insight, it is useful to directly compare observations with 1-D calculations. While it is not feasible to use the spatial autocorrelation function for this purpose, a suitable alternative is to use the shortwave reflectance standard deviation. Using the same approach as outlined in the previous sections, observed and calculated reflectance standard deviations are compared for reciprocal pairs as functions of μ and μ_0 (all pixels were degraded to the resolution at $\mu = 0.35$). The standard deviations are inferred directly from the distribution of reflectances in each angular bin. For the calculations, 1-D reflectances are calculated from pixel-level cloud fraction—cloud optical depth pairs inferred at nadir for $\mu_0 = 0.9 - 1.0$.

Results of this comparison are provided in Figure 12, which shows observed and plane parallel model reflectance standard deviations for the reciprocal sets of angles at $\mu = 0.9-1.0$ as a function of μ_0 and $\mu_0 = 0.9-1.0$ as a function of μ in the backscattering direction. Note that in the latter case, standard deviations could be obtained only for $\mu > 0.3$ since beyond this point, the observations are unreliable. As shown, the observed standard deviations for the reciprocal pairs are quite different, whereas the calculated values are virtually identical (a slight difference in the calculated values occurs because of minor differences in the R^{CLR} values).

Observed standard deviations are found to exceed the corresponding plane parallel values in all cases. Interestingly, the largest deviation from 1-D theory occurs in the nadir observations for different μ_0, and these differences become progressively larger as μ_0 decreases.

Thus, when scenes containing clouds are illuminated obliquely and observed at nadir at ERBS pixel scales, the statistical properties in the reflectance field appear to be more sensitive to horizontal inhomogeneities than when the same scenes are viewed obliquely for overhead Sun. Consequently, the main reason for the breakdown in directional reciprocity in the ERBS observations is because of the difference in the way observed reflectances depend on μ_0, compared with 1-D theory.

4. Discussion

Overall, results presented in this study are largely consistent with earlier theoretical studies of cloud heterogeneity. For Sun angles close to zenith, Kobayashi [1993] showed that differences between 3-D and plane parallel cloud reflectances tend to be smaller at oblique view angles than at nadir, due mainly to diffuse leakage of radiation out the sides of clouds. This is consistent with the excellent agreement between plane parallel reflectances and observed reflectances at oblique views for high Sun elevations. Agreement at nadir view must, of course, be discounted since it was these views that were used to normalize the plane parallel models. At smaller μ_0, the tendency for reflectance differences to increase is also apparent in theoretical studies [e.g., Davies, 1984; Bréon, 1992; Kobayashi, 1993]. In the backscattering direction, these studies have shown that 3-D clouds tend to scatter more radiation owing to the presence of cloud sides. In the forward scattering direction, the tendency for plane parallel model reflectances to be larger

than the observations at small μ is also qualitatively consistent with 3-D theory. *Stuhlmann et al.* [1985] came to a similar conclusion when they compared 1-D and Nimbus 7 Earth Radiation Budget (ERB) cloud anisotropic functions.

The lack of any μ dependence in the difference between observed and plane parallel reflectances in the backscattering direction is unexpected, however. While this behavior is consistent with theoretical results for clouds of low aspect ratio, it is not what we would expect of vertically extensive 3-D clouds. In the latter case, the increase in reflectance with view angle is generally much stronger than shown by the present observations. The reason for this discrepancy is unclear. While it may be tempting to conclude that real clouds viewed obliquely at low spatial resolutions behave more like horizontally extensive layers, this is not what we expect of the tropical clouds composing our data set. *Rossow* [1989] noted that since the pixel size is of order of or greater than the path length of visible radiation, multiple scattering within and between clouds may eliminate most of the deviations from 1-D behavior. This also is an unlikely explanation since average cloud fractions in the present study are estimated to be low (≈ 0.4), so that multiple scattering between clouds is likely to be quite small, on average. Another possible reason may be associated with the absorption properties of clouds. Recent studies have speculated that theoretical models may actually be underestimating cloud absorption [*Stephens and Tsay*, 1990; *Cess et al.*, 1995]. While stronger absorption could lead to a weaker view angle dependence in the reflectance field, there is no observational evidence to support that this is happening.

5. Summary and Conclusions

Broadband reflectances derived from plane parallel theory have been directly compared with 1 year of ERBS scanner measurements over ocean equatorward of 30° as a function of view, solar zenith, and relative azimuth angle. The calculations were normalized to the observations on a pixel-by-pixel basis at nadir and $\mu_0 = 0.5 - 0.6$, $0.7 - 0.8$, and $0.9 - 1.0$ by inferring combinations of cloud fraction and cloud optical depth which ensured a match at these angles.

On average, the μ dependence from plane parallel theory was consistent with the observations at moderate to high Sun elevations ($\mu_0 > 0.4$). At lower Sun elevations, observed reflectances tended to exceed plane parallel model values in the backscattering direction, with (absolute) differences ranging from less than 2% at intermediate μ_0 to as much as 10% at the most oblique Sun angles. Provided the atmosphere above the cloud was accounted for, no systematic μ dependence in the difference was observed in the backscattering direction, on average. In the forward scattering direction, plane parallel model reflectances were more sensitive to the model assumptions (such as cloud top height, subpixel

cloud fraction), and consequently, observed reflectances generally fell within the range of plane parallel model values. Despite this, there were significant differences at small μ; observed reflectances leveled off between $\mu = 0.5$ and 0.3, whereas the calculations increased steadily.

When stratified by pixel brightness, the plane parallel model approximation provided a better approximation to the observed reflectance dependence on μ for darker (i.e., optically thinner) pixels than for brighter (optically thicker) pixels. Reflectance differences were also found to be less sensitive to pixel brightness at oblique view angles in the backscattering direction than at nadir. Relative differences were generally $\lesssim 5\%$ at oblique view angles for $\mu_0 > 0.45$ and were $\lesssim 20\%$ at smaller μ_0. When compared as a function of relative azimuth angle, both model and observations showed a similar relative dependence on angle. Neglecting pixel area expansion with view angle in the calculations was shown to have only a minor influence.

Finally, in order to further examine use of the principle of directional reciprocity to satellite measurements at ERBS pixel spatial scales, reflectance standard deviations from 1 year of observations and plane parallel calculations were compared for the reciprocal sets of angles at $\mu = 0.9-1.0$ as a function of μ_0 and $\mu_0 = 0.9-1.0$ as a function of μ in the backscattering direction. These comparisons showed that the main reason for the breakdown in directional reciprocity in ERBS observations is due to the systematic difference in the reflectance dependence on solar zenith angle between observations and 1-D theory. At low Sun, observed standard deviations were found to be much larger than those predicted by 1-D theory, suggesting that the breakdown in directional reciprocity is likely associated with an increase in scene complexity (or horizontal inhomogeneity) under these viewing conditions and spatial scales.

References

Aida, M. A., Scattering of solar radiation as a function of cloud dimension and orientation, *J. Quant. Spectrosc. Radiat. Transfer, 17,* 303–310, 1977.

Bohren, C. F., and D. R. Huffman, *Absorption and Scattering of Light by Small Particles,* 530 pp., John Wiley, New York, 1983.

Bréon, F.-M., Reflectance of broken cloud fields: Simulation and parameterization, *J. Atmos. Sci., 49,* 1221–1232, 1992.

Busygin, V. P., N. A. Yevstratov, and Y. M. Feigel'son, Optical properties of cumulus clouds, and radiant fluxes for cumulus cloud cover, *Izv. Acad. Sci. USSR Atmos. Oceanic Phys.,* Engl. Transl., *9,* 1142–1151, 1973.

Cess, R. D., et al., Absorption of solar radiation by clouds: Observations versus models, *Science, 267,* 496–499, 1995.

Chandrasekhar, S., *Radiative Transfer*, 393 pp., Oxford Univ. Press, New York, 1950.

Coakley, J. A., Reflectivities of uniform and broken layered clouds, *Tellus, Ser. B, 43B*, 420–433, 1991.

Davies, R., The effect of finite geometry on the three-dimensional transfer of solar irradiance in clouds, *J. Atmos. Sci., 35*, 1712–1725, 1978.

Davies, R., Reflected solar radiances from broken cloud scenes and the interpretation of scanner measurements, *J. Geophys. Res., 89*, 1259–1266, 1984.

Davies, R., Spatial autocorrelation of radiation measured by the Earth Radiation Budget Experiment: Scene inhomogeneity and reciprocity violation, *J. Geophys. Res., 99*, 20,879–20,887, 1994.

Deirmendjian, D., *Electromagnetic Scattering on Spherical Polydispersions*, 290 pp., Elsevier, New York, 1969.

Hale, G. M., and M. R. Querry, Optical constants of water in the 200-nm to 200μm wavelength region, *Appl. Opt., 12*, 555–563, 1973.

Kobayashi, T., Effects due to cloud geometry on biases in the albedo derived from radiance measurements, *J. Clim., 6*, 120–128, 1993.

Kopia, L. P., The Earth Radiation Budget Experiment Scanner instrument, *Rev. Geophys., 24*, 400–406, 1986.

Loeb, N. G., and R. Davies, Observational evidence of plane parallel model biases: The apparent dependence of cloud optical depth on solar zenith angle, *J. Geophys. Res., 101*, 1621–1634, 1996.

McKee, T. B., and S. K. Cox, Scattering of visible radiation by finite clouds, *J. Atmos. Sci., 31*, 1885–1892, 1974.

Minnis, P., Viewing zenith angle dependence of cloudiness determined from coincident GOES east and GOES west data, *J. Geophys. Res., 94*, 2303–2320, 1989.

Rossow, W. B., Measuring cloud properties from space: A review, *J. Clim., 2*, 201–213, 1989.

Stamnes, K., S.-C. Tsay, W. Wiscombe, and K. Jayaweera, Numerically stable algorithm for discrete-ordinate-method radiative transfer in multiple scattering and emitting layered media, *Appl. Opt., 24*, 2502–2509, 1988.

Stephens, G. L., and S.-C. Tsay, On the cloud absorption anomaly, *Q. J. R. Meteorol. Soc., 116*, 671–704, 1990.

Stuhlmann, R. S., P. Minnis, and G. L. Smith, Cloud bidirectional reflectance functions: A comparison of experimental and theoretical results, *Appl. Opt., 24*, 396–401, 1985.

Wielicki, B. A., and R. N. Green, Cloud identification for ERBE radiative flux retrieval, *J. Appl. Meteorol., 28*, 1133–1146, 1989.

Wielicki, B. A., and L. Parker, On the determination of cloud cover from satellite sensors: The effect of sensor spatial resolution, *J. Geophys. Res., 97*, 12,799–12,823, 1992.

Ye, Q., and J. A. Coakley Jr., Biases in earth radiation budget observations, 1, Effects of scanner spatial resolution on the observed anisotropy, *J. Geophys. Res., 101*, 21,243–21,252, 1996a.

Ye, Q., and J. A. Coakley Jr., Biases in earth radiation budget observations, 2, Consistent scene identification and anisotropic factors, *J. Geophys. Res., 101*, 21,253–21,263, 1996b.

R. Davies, Institute of Atmospheric Physics, The University of Arizona, P. O. Box 210081, Tucson, AZ 85721-0081. (e-mail: davies@air.atmo.arizona.edu)

N. G. Loeb, College of Oceanic and Atmospheric Sciences, Oregon State University, Corvallis, OR 97331.